Journal of the Optical Society of America A
OPTICS, IMAGE SCIENCE, AND VISION

Focus correction in an apodized system with spherical aberration

PAULA BERNAL-MOLINA,[1] JOSÉ FRANCISCO CASTEJÓN-MOCHÓN,[2] ARTHUR BRADLEY,[3] AND NORBERTO LÓPEZ-GIL[1,*]

[1]Laboratorio Interuniversitario de Investigación en Visión y Optometría, Universidad de Murcia, 30100 Murcia, Spain
[2]Departamento de Ciencias Politécnicas, Universidad Católica San Antonio, 30107 Murcia, Spain
[3]Indiana University School of Optometry, Bloomington, Indiana 47405, USA
*Corresponding author: norberto@um.es

Received 24 April 2015; revised 1 July 2015; accepted 4 July 2015; posted 6 July 2015 (Doc. ID 239680); published 24 July 2015

We performed a theoretical and computational analysis of the through-focus axial irradiance in a system with a Gaussian amplitude pupil function and fourth- and sixth-order spherical aberration (SA). Two cases are analyzed: low aberrated systems, and the human eye containing significant levels of SA and a natural apodization produced by the Stiles–Crawford effect. Results show that apodization only produces a refraction change of the plane that maximized the Strehl ratio for eyes containing significant levels of negative SA.

OCIS codes: (330.0330) Vision, color, and visual optics; (330.4595) Optical effects on vision; (330.4875) Optics of physiological systems; (220.1230) Apodization; (220.1010) Aberrations (global).

http://dx.doi.org/10.1364/JOSAA.32.001556

1. INTRODUCTION

Amplitude filtering is a technique usually used to improve the quality of images formed by an optical system [1]. Diffractive effects may be avoided partially by means of this technique, increasing the system resolution ("super-resolution") at the expense of a decrease in the energy transmitted [2]. Apodization, one type of amplitude filtering, is also broadly used when using lasers with Gaussian beams [3], and, in astronomy, when trying to avoid the undesirable effects of a bright star on planets with low intensity located in its vicinity [4].

Most instrument optical systems, and especially telescopes with large apertures, are corrected for spherical aberration (SA) by using either aspheric lenses or combinations of lenses with different amounts of SA designed to cancel each other's SA, such as a Schmidt camera [5]. Total cancellation is difficult to achieve, and, although it may be achieved for a certain target, it will be imperfect for objects placed at other distances (see Chapter 5 in [6]).

In this context, it is useful to know the defocus that can maximize the image irradiance of a point source produced by a system with an amplitude filter and a certain amount of SA. The human eye exhibits a significant Gaussian amplitude filter (the Stiles–Crawford effect (SCE) apodization [7]) and significant levels of SA (more than typically encountered in fabricated optical systems [8]). In addition, identifying the defocus term that can maximize image quality in the human eye is a most critical clinical task, which has been shown to vary with both SA and apodization levels [9,10]. Extreme cases exist in eyes that have undergone corneal refractive surgery [11] and eyes implanted with refractive multifocal IOLs or with multifocal contact lenses for presbyopia correction. The vision of these subjects is known to deteriorate with larger pupil sizes (typically found in night conditions) [12,13]. The change in refractive state that accompanies elevated levels of SA [10] is one possible reason for reduced visual performance. Therefore, the best refraction correction used during the day may not be the best to use at night [14].

We performed a theoretical analysis of the axial point spread function (PSF) irradiance in a system with SA and a Gaussian apodized pupil function. Refractive error was determined by the defocus that maximized the Strehl ratio (SR). This study reveals changes in the refractive state of the eye caused by typical values of SA and SCE.

2. METHODS

We assume an optical system with a radial symmetrical wavefront that includes a certain value of defocus A_d, primary (SA4) A_s, and secondary (SA6) B_s SA [15]:

$$W = A_d\rho^2 + A_s\rho^4 + B_s\rho^6. \quad (1)$$

Considering that the transmittance amplitude of the system is apodized and both SA values are constant, our goal was to find the defocus value, A_d, which, when added to the wavefront, will maximize the SR (see Chapter 9 in [6]).

The normalized irradiance at a certain point P in the image plane created by an optical system with a wave aberration, W,

and a circular normalized pupil with an exponential apodization factor, γ, can be written as [5,15]

$$I_P = \frac{1}{\pi^2}\left|\int_0^{2\pi}\int_0^1 \exp(-\gamma\rho^2)\exp(ikW)\rho\mathrm{d}\rho\mathrm{d}\theta\right|^2. \quad (2)$$

Then, for $\gamma = 0$, we have a binary pupil (no apodization), and, when γ is a large value, the apodization follows a narrow Gaussian shape.

From Eq. (2),

$$\begin{aligned} I_P &= \frac{1}{\pi^2}\left|\int_0^{2\pi}\int_0^1 \exp(-\gamma\rho^2)(1 + ikW \right. \\ &\quad \left. + \frac{1}{2}(ikW)^2 + \cdots)\rho\mathrm{d}\rho\mathrm{d}\theta\right|^2 \\ &= \frac{1}{\pi^2}\left|\int_0^{2\pi}\int_0^1 \exp(-\gamma\rho^2)\rho\mathrm{d}\rho\mathrm{d}\theta \right. \\ &\quad + \int_0^{2\pi}\int_0^1 \exp(-\gamma\rho^2)ikW\rho\mathrm{d}\rho\mathrm{d}\theta \\ &\quad \left. + \int_0^{2\pi}\int_0^1 \exp(-\gamma\rho^2)\frac{1}{2}(ikW)^2\rho\mathrm{d}\rho\mathrm{d}\theta + \ldots\right|^2. \quad (3) \end{aligned}$$

Knowing that [15]

$$\begin{aligned} \langle W^n\rangle &= \frac{\int_0^1\int_0^{2\pi}[W(\rho,\theta)]^n\exp(-\gamma\rho^2)\rho\mathrm{d}\rho\mathrm{d}\theta}{\int_0^1\int_0^{2\pi}\exp(-\gamma\rho^2)\rho\mathrm{d}\rho\mathrm{d}\theta} \\ &= \frac{\Gamma}{\pi}\int_0^1\int_0^{2\pi}[W(\rho,\theta)]^n\exp(-\gamma\rho^2)\rho\mathrm{d}\rho\mathrm{d}\theta, \quad (4) \end{aligned}$$

with

$$\Gamma = \frac{\gamma}{[1-\exp(-\gamma)]}. \quad (5)$$

Equation (3) can be rewritten as

$$\begin{aligned} I_P &= \frac{1}{\pi^2}\left|\frac{\pi}{\Gamma} + \frac{\pi}{\Gamma}ik\langle W\rangle + \frac{1}{2}\frac{\pi}{\Gamma}(ik)^2\langle W^2\rangle + \ldots\right|^2 \\ &= \frac{1}{\Gamma^2}\left|1 + ik\langle W\rangle - \frac{1}{2}k^2\langle W^2\rangle + \ldots\right|^2. \quad (6) \end{aligned}$$

In the following, we employ Eq. (6) to examine two kinds of optical systems: those with small amounts of aberrations and those that are highly aberrated. We consider a system to have small aberrations if it meets the Maréchal criterion [16]. This criterion requires the standard deviation (RMS) to be less than $\lambda/10$ [although the value $\lambda/14$ is usually used (see Chapter 9 in [6])]. This means that RMS has to be less than 0.055 μm to be considered a low aberrated wavefront.

A. Systems with Small Aberrations

For small aberrations, Eq. (6) can be approximated to (see Chapter 9 in Ref. [6]) [6,15]

$$I_P \approx \frac{1}{\Gamma^2}\left|1 + ik\langle W\rangle - \frac{1}{2}k^2\langle W^2\rangle\right|^2 = \frac{1}{\Gamma^2}(1 - k^2\sigma_W^2), \quad (7)$$

where σ_W^2 is the variance of the wavefront defined as

$$\sigma_W^2 = \langle W^2\rangle - \langle W\rangle^2. \quad (8)$$

Equation (7) shows the classic relation between axial irradiance and wavefront variance in a low aberrated system (see Chapter 9 in Ref. [6]) [6,15], but multiplied by a factor that takes into account the apodization. This result also shows that I_P is maximum when σ_W^2 is minimum (see Chapter 9 in Ref. [6]) [6,15].

To find the value of the defocus A_d that minimizes the variance of a wavefront, the following equation must be solved:

$$\frac{\partial\sigma_W^2}{\partial A_d} = \frac{\partial(\langle W^2\rangle - \langle W\rangle^2)}{\partial A_d} = 0. \quad (9)$$

Equation (4) can be rewritten as

$$\langle W^n\rangle = 2\Gamma\int_0^1 [W(\rho)]^n\exp(-\gamma\rho^2)\rho\mathrm{d}\rho, \quad (10)$$

and, following Eqs. (1), (9), and (10), the equations to solve are

$$\langle W\rangle^2 = \left[2\Gamma\int_0^1 [A_d\rho^2 + B_s\rho^4 + B_s\rho^6]\exp(-\gamma\rho^2)\rho\mathrm{d}\rho\right]^2, \quad (11)$$

$$\langle W^2\rangle = 2\Gamma\int_0^1 [A_d\rho^2 + B_s\rho^4 + B_s\rho^6]^2\exp(-\gamma\rho^2)\rho\mathrm{d}\rho. \quad (12)$$

As a result, we found that the defocus that maximizes the irradiance is then given by

$$A_d = \frac{A_s(\xi - 2\Gamma\alpha\eta) + B_s(\tau - 2\Gamma\alpha\xi)}{2\Gamma\alpha^2 - \eta}. \quad (13)$$

All calculations and definitions of values α, η, ξ, and τ in Eq. (13) are defined in Appendix A. When there is no apodization ($\gamma = 0$), Eq. (13) gives the known value [17]

$$A_d = -A_s - 9/10B_s. \quad (14)$$

B. Systems with Large Aberrations

The approximation made in Eq. (7) for small aberrations (typically found in many fabricated optical systems) cannot be applied in optical systems with large amounts of aberration, such as the human eye (since, in a study performed in a population of 2,560 normal eyes, the mean value of the RMS for third- to fifth-order Zernike aberrations was 0.186 ± 0.078 μm for a 5 mm pupil [18], much more than the value established by Maréchal criterion). This indicates that the A_d value in Eq. (13) could not maximize the irradiance at the image plane. This fact explains why the Zernike metric does not give the same values as the SR metric in the human eye [19].

An exact analytical solution of Eq. (2) can be calculated when considering a wavefront with only fourth-order SA ($W = A_d\rho^2 + A_s\rho^4$):

$$\begin{aligned} I_P &= \frac{1}{\pi^2}\left|\int_0^{2\pi}\int_0^1 \exp(-\gamma\rho^2)\exp(ik(A_d\rho^2 + A_s\rho^4))\rho\mathrm{d}\rho\mathrm{d}\theta\right|^2 \\ &= \left|\frac{\exp(a+b)F\left(\frac{a+2b}{2\sqrt{b}}\right) - F\left(\frac{a}{2\sqrt{b}}\right)}{\sqrt{b}}\right|^2, \quad (15) \end{aligned}$$

where $F(z)$ is the Dawson integral [20], $a = (ikA_d - \gamma)$ and $b = ikA_s$. When considering a wavefront with both SA4 and SA6, an exact solution for Eq. (2) cannot be found. Instead, it is calculated numerically.

3. RESULTS

Figure 1 shows the irradiance axial distribution ($\lambda = 0.555$ μm, $k = 2\pi/\lambda = 11.32$ μm^{-1}) for three values of SA (A_s) corresponding to (a) an eye with lower than average SA; (b) an eye containing the mean SA found in normal eyes [18]; and (c) a myopic post-LASIK eye with almost four times the normal levels of positive SA [21] (negative A_s values are found in hyperopic post-LASIK eyes). Figures were computed for $\gamma = 0$ (no SCE) and $\gamma = 0.5$, corresponding to the normal value of the directionality parameter, $\rho = 0.055/\text{mm}^2$ for a 6 mm pupil [22,23].

Through-focus curves may have more than one maximum [see, for instance, Fig. 1(b), without SCE]. In this case, we identify the best refraction with the maximum with the less negative (more positive) A_d value, which is indicated with black arrows in Fig. 1. The reason for this choice is based on the criteria normally used during a typical clinical refraction: when two refractions give the same optical performance, the more positive refraction (more positive A_d) is selected. This criterion assures the maximum possible interval of clear vision for the subject by placing the eye's far point at the infinity.

Figure 2 shows the irradiance axial distribution obtained for the same parameters as Fig. 1, but includes a value of SA6 corresponding to $B_s = 0.5$ μm (0.90λ) (the corresponding Zernike coefficient $C_6^0 = 0.0094$ μm (0.017λ) can be computed from Eq. (4) in Ref. [17]). This value is about 2.5 times

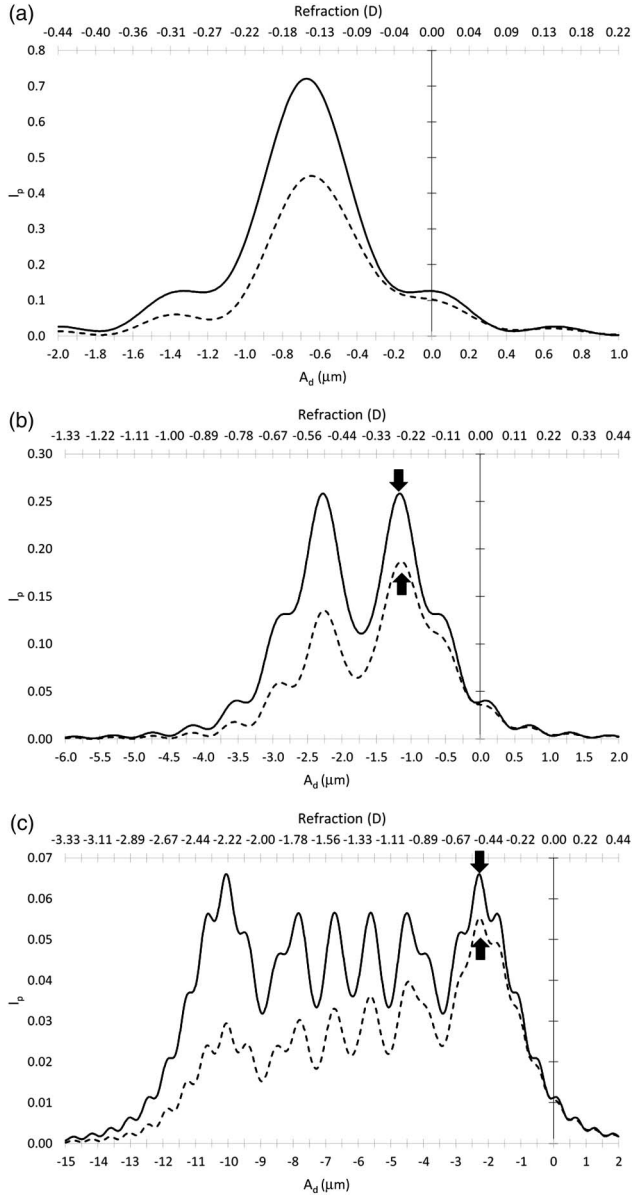

Fig. 1. Axial intensity in the image plane. Black line, without apodization ($\gamma = 0$); dashed line, with apodization ($\gamma = 0.5$). Arrows in the figures indicate the expected clinical refraction. Figures A, B, and C correspond to A_s values of 0.67 μm (1.21λ), 1.72 μm (3.10λ), and 6.17 μm (11.12λ), respectively.

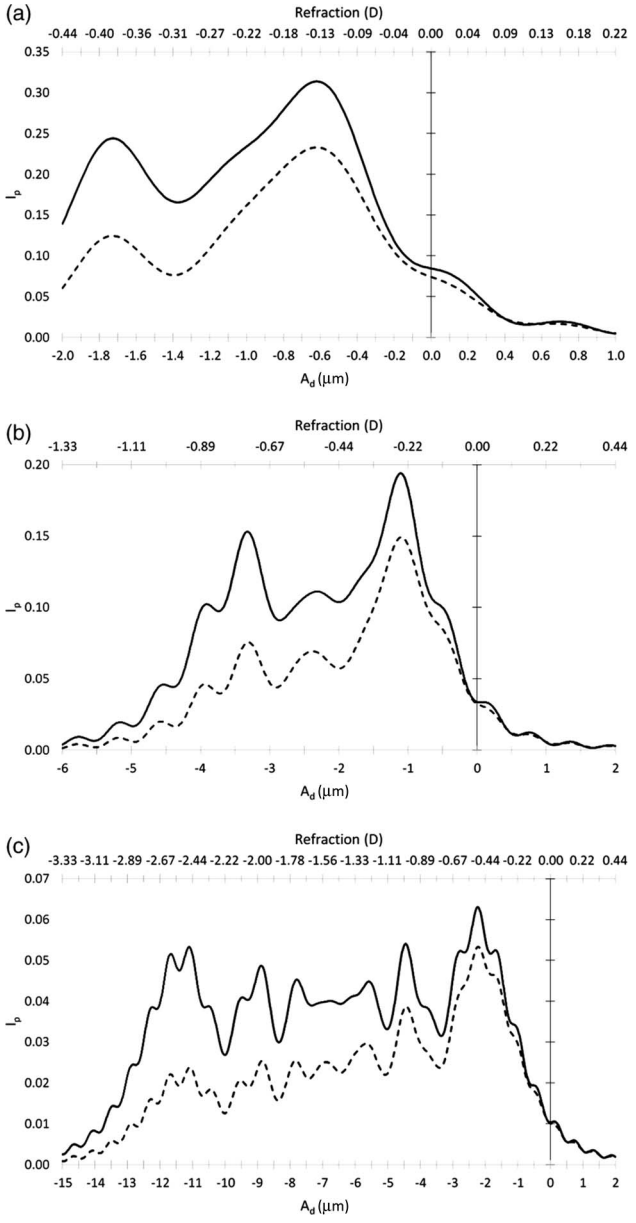

Fig. 2. Axial intensity in the image plane for a wavefront with sixth-order SA ($B_s = 0.5$ μm $= 0.90\lambda$), and several values of fourth-order SA: (a) $A_s = 0.67$ μm $= 1.21\lambda$, (b) $A_s = 1.72$ μm $= 3.10\lambda$, and (c) $A_s = 6.17$ μm $= 11.12\lambda$. Black line, without apodization ($\gamma = 0$); dashed line, with apodization ($\gamma = 0.5$).

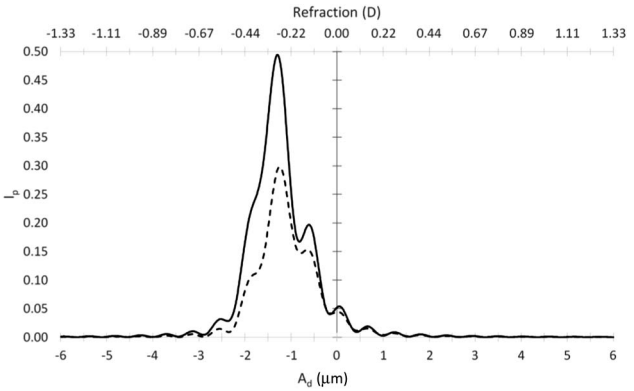

Fig. 3. Axial intensity in the image plane for a wavefront, including both the fourth- and sixth-order SAs with opposite signs (A_s = 1.72 μm = 3.10λ and B_s = –0.5 μm = –0.90λ). Black line, without apodization ($\gamma = 0$); dashed line, with apodization ($\gamma = 0.5$).

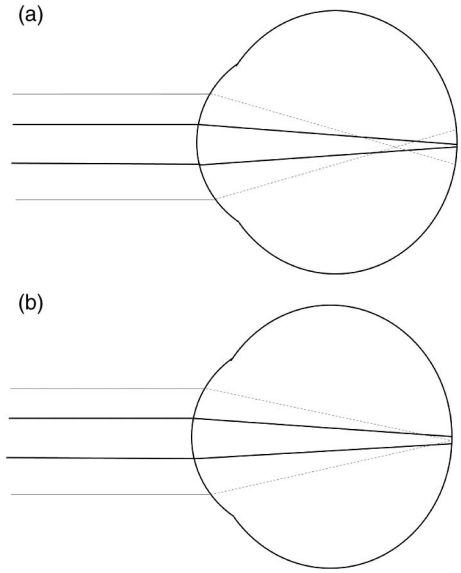

Fig. 4. Schematic ray tracing for paraxial (black) and peripheral (gray dotted) rays in an eye with positive SA. SCE has a larger effect on peripheral rays for (a) $A_d < 0$ than for (b) $A_d \ll 0$.

smaller than the mean value present in the unaccommodated eye [18].

The presence of an SA6 breaks the symmetry shown in Fig. 1 when no apodization is presented, and decreases the through-focus irradiance values.

Figure 3 shows the results obtained when combining opposite signs SA4 and SA6 in the case of Fig. 2(b) [A_s = 1.72 μm (3.10λ) and B_s = –0.5 μm (–0.90λ)]. In this case, the through-focus plots show a significantly reduced depth of field (DoFi), but an increase of the I_p with or without SCE.

4. DISCUSSION

For fabricated optical systems with large apertures and low aberrations, such as telescopes, the presence of some SA and an amplitude filter may slightly alter the defocus value that produces the highest irradiance of the image of a point source. Equation (13) gives the exact analytical solution which depends on the Seidel SA values, A_s and B_s, and the apodization parameter, γ.

For optical systems with relatively high levels of aberration, such as the human eye, with an apodization value of $\gamma = 0.5$ for a 6 mm pupil, our analytical methods can find the expected decrease in the maximum axial irradiance, as well as the shift of the through-focus curve toward negative values of A_d, as A_s increases (Fig. 1). Figure 4 shows schematically where rays passing through the center or the edge of the pupil focus for two values of A_d, corresponding to (a) the first maximum (less negative value of A_d) and (b) the second maximum in Fig. 1(b) that has a certain positive value of SA4. The shift is because the annular areas in the periphery of the pupil, which have a larger positive power (dashed lines in Fig. 4), are better focused in the presence of a negative defocus, and the SCE reduces their effect by giving a larger weight to the light passing through the central part of the pupil. When the pupil margins are focused [Fig. 4(b)], there is less light contributing to the central image irradiance, reducing the SR [e.g., Fig. 1(c), second maximum]. With negative SA4, the effect of the SCE is the opposite; the attenuated maximum is that for the most positive A_d value [Fig. 5(a)].

For certain values of A_s, though-focus curves may present more than one maximum with the same irradiance [e.g., Fig. 1(b)]. Thus, as indicated by Figs. 1(b) and 1(c), a negligible refractive change might be expected to be produced by the SCE. In terms of diopters, the change in refraction can be calculated using the relation $R_x = 2 \cdot A_d/(\text{pupil radius})^2$. In the three cases shown in Fig. 1, the refractive shifts are –0.006D [A_s = 0.67 μm (1.21λ)), Fig. 1(a)], –0.005D [A_s = 1.72 μm (3.10λ), Fig. 1(b)], and –0.004D [A_s = 6.17 μm (11.12λ), Fig. 1(c)]. In the presence of SA6, no refractive change is produced, as is shown in Fig. 2. Computer simulations of the retinal image have recently confirmed these results [24].

The effect of the presence of SA6 in the wavefront is shown when comparing Figs. 1 and 2. The symmetry around $A_d = -A_s$ for $\gamma = 0$ found in Fig. 1 is absent if SA6 is present. In addition, the through-focus irradiance values decrease when the wavefront is formed by primary and secondary SA with the same sign. Comparing Figs. 2(b) and 3, we can see the effect of the opposite sign in SA4 and SA6.

The second maximum peak shown in Fig. 2(b) is strongly attenuated, while the principal maximum increases by about 2.5 times, with respect to the highest value obtained when there is no SA6. This interesting result shows the connection between SA4 and SA6 in terms of SR. This relation has been studied recently by means of numerical calculations [10]. After the appropriated defocus correction, SA6 may flatten the wavefront generated by the opposite sign SA4, thus increasing the concentration of light in the image plane [25,26]. This effect may already be anticipated, taking into account the presence of SA4 and SA6 with the opposite sign in the definition of the Zernike's sixth-order SA polynomial (see Chapter 9 in [6]). The proportionality between SA4 and SA6 (three parts of SA4 for two of SA6) given by the sixth-order SA Zernike

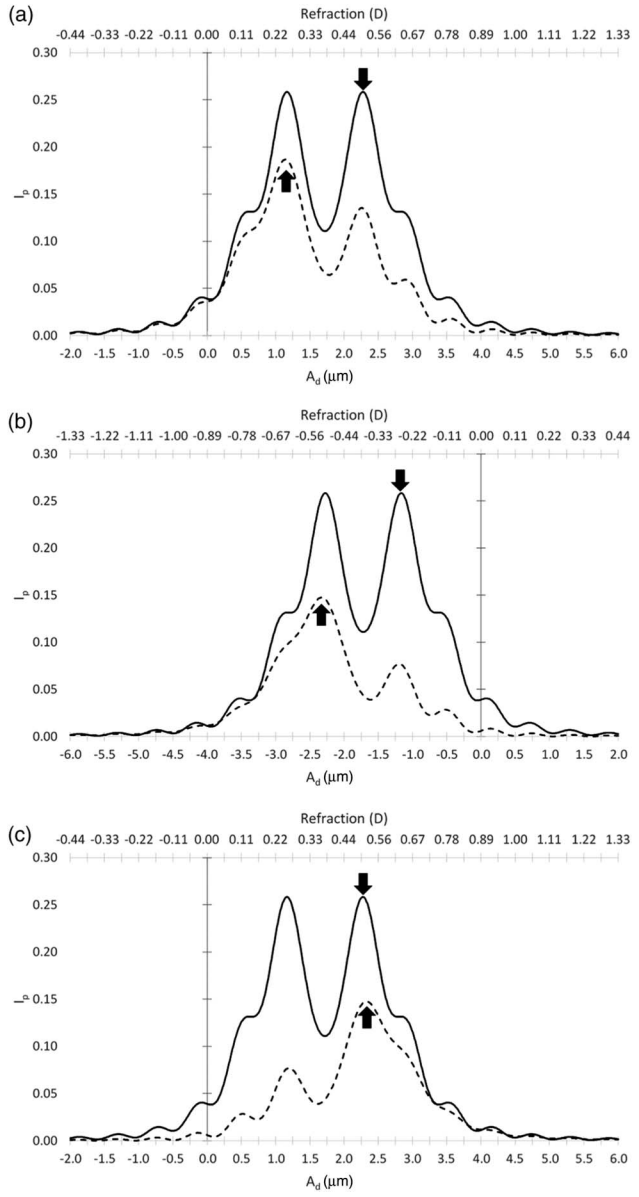

Fig. 5. (a) SCE and $A_s = -1.72$ μm (-3.10λ), (b) reversal SCE and $A_s = 1.72$ μm (3.10λ), and (c) reversal SCE and $A_s = -1.72$ μm (-3.10λ). Arrows in the figures indicate the clinical refraction. Black line, without apodization ($\gamma = 0$); dashed line, with apodization ($\gamma = 0.5$).

polynomial, which minimizes RMS, does not appear to be the best ratio SA4/SA6 to maximize resolution in the human eye [24].

When A_s and B_s change their signs simultaneously, the I_p through-focus curves are mirror-symmetric with respect to the y axis [the integral in Eq. (2) gives the same value, changing A_d by just $-A_d$] [27]. Figure 5 shows this effect.

In this case, normal apodization ($\gamma > 0$) could affect the refractive state of the eye, since the principal maximum will retain the lower value of A_d. In optical terms, the reduction of the intensity of the rays passing closer to the edge of the pupil mainly affects the maximum produced for a value of A_d which focuses the marginal optics. This is not the A_d determined by a clinical refraction of an eye with +SA and $+\gamma$ (see Fig. 1), but corresponds to the defocus selected in clinical refraction when SA is negative, as can occur in the accommodated eye [17], or in highly myopic eyes fit with negative contact lenses [28] and post-refractive surgery eyes that have been corrected for hyperopia [29].

An interesting case would appear for a reversal SCE ($\gamma < 0$), with an amplitude function $e^{-\gamma\rho^2} + 1 - e^{-\gamma}$, that assures a transmittance of 100% at the edge of the pupil, $\rho = 1$ [10,30]. Figure 5(b) shows this case for $A_s > 0$. In this hypothetical case, we can expect a change in the clinical refractive state of the eye since apodization affects the more positive maximum of the I_p through-focus curve. That is, rays passing through the edge of the pupil, which are more efficient and more powered, concentrate in front of the retina, producing a myopic focus, and, thus, requiring a myopic shift in the correction.

Then, in the presence of only SA4, our results indicate that refractive changes (following the clinical "maximum plus" procedure [31]) are found when A_s and γ-values have the opposite sign.

Figure 6 shows the refractive state as a function of SA4 with or without SCE ($\gamma = 0.5$). The refractive state was calculated as the defocus value computed using two different strategies: (1) minimizing the variance of the wavefront, min RMS [Eq. (9)] and (2) maximizing the irradiance I_p (maximizing the SR) given in Eq. (14). The range of A_s used in Fig. 6 includes low values of A_s usually present in fabricated optical systems, and high values typically found in post-LASIK eyes, e.g., up to values of $A_s = 6.17$ μm (11.12λ) for a 6 mm pupil [21].

Figure 6 shows that, for a system with low aberrations [A_s values up to ±0.5 μm ($\pm 0.90\lambda$)], minimizing variance or maximizing SR gives the same result, as expected from Eq. (7) [32]. For positive values of A_s, there is also no change in the refraction produced by SCE for both metrics. However, Fig. 6 shows that, for negative values of A_s lower than −0.5 μm (-0.90λ), the SR metric produces a change in the clinical refractive error in the presence of SCE. Adding a centrally weighted pupil amplitude function will always reduce the intensity of marginal rays, and, thus, the image irradiance peak generated when the pupil margin is focused. For an eye with

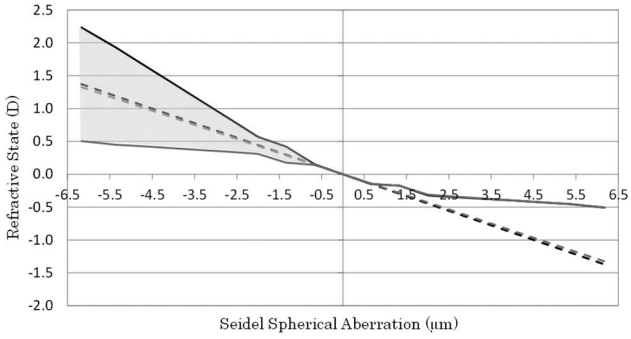

Fig. 6. Refractive state as a function of primary SA, computed for the minimum RMS criterion (dotted line) without SCE (black) and with SCE (gray); and for maximizing the SR (solid line) without SCE (black) and with SCE (gray). Apodization factor used is $\gamma = 0.5$. Shaded area shows the refractive change produced by considering the SCE.

+SA, this attenuated peak exists at the most negative focus, which is not used clinically. However, in the presence of negative SA, the marginal focus is created with plus A_d, and, therefore, reducing this most positive peak in the through-focus plot removes the peak we typically select when doing clinical spherical refractions. The apodization effect in the refractive state obtained with the SR metric increases when the negative value of SA4 increases, and, thus, may be important in post-hyperopic-LASIK eyes. The effective refractive state of a SA < 0 is, in terms of the SR metric, much lower in the presence of SCE (Fig. 6). Indeed, Fig. 6 shows a similar tendency to the one obtained using the metric VSOTF [24].

These results may explain the experimental observations showing that SCE plays a small role in the refraction in the presence of positive SA [18,33,34], typically found in the relaxed human eye [17]. The results also explain why, for negative SA (typically presented in accommodated eyes), which produces an image with a minimum RMS behind the retina, the visual system does not need to accommodate perfectly (accommodative lag).

Results for low values of SA (Fig. 6) also agree with experimental measurements, which indicate that the visual system can effectively employ a refraction based on minimum RMS (Zernike [35]) refraction [32]. However, Zernike refractions do not seem to be a good representative of subjective refraction for larger values of SA [9,10,32], since they will introduce myopic or hyperopic biases to the refractive state in the presence of +SA or –SA, respectively. Instead, the maximum SR observed with SA and SCE better matches the subjective refractive change produced by the presence of SA [10].

The relatively simple analytical formulation presented in this paper can be used in any fabricated rotationally symmetric optical system with Gaussian apodization, usually with low values of SA. It is also a mathematical tool to perform further studies of refraction in aberrated eyes. Another potential field of application that has not been explored in this study is the use of an induced SA, together with a certain apodization, to maximize the eye's DoFi, which may partially avoid the effects of presbyopia. The extension of the through-focus curves may be related to this value. In this regard, some experimental studies have already been performed by inducing SA4 and SA6 in the form of the Zernike polynomials, Z_4^0 and Z_6^0 [25,26]. A recent experimental study has also shown the potential benefits of the apodization in the DoFi [36].

Taking all this into account, we are aware of the limitations of the applications of our results on visual optics mainly for three reasons. First, our study has focused on just two symmetrical high-order aberrations, primary and secondary SA. The presence of other aberrations would certainly vary the through-focus curves [24]. Second, we have not taken into account the presence of chromatic aberration. This limitation may be overcome, knowing the spectral apodization factor and performing the same calculations for different wavelengths that are finally added together [37]. Third, our study assumes that maximizing the irradiance of the retinal image of a point source (SR metric [38]) may be a good refraction metric, which cannot be totally true since it does not take into account the additional visual effects produced by the neural system. However, neutrally weighting the SR metric failed to improve its accuracy at predicting spherical refractions, and actually decreased it a little [19,39] in daylight conditions. Nevertheless, our study expands the SR metric to a more complex metric that includes the neural factor related to the SCE. This metric should be of interest, for instance, to astronomers who are interested in maximizing the detection of dim stars [14].

In conclusion, in our study we find an expression for the focal shift that maximizes the irradiance in a general optical system with apodization and SA. This focal shift is normally small (thousandths of a diopter), even for a large value of apodization. The application to the human eye shows that the apodization created by the SCE plays a small role in the refractive change, unless the eye has a relatively large value of fourth-order negative SA and a maximum plus clinical criterion when refracting the eye is used.

APPENDIX A

This appendix shows the resolution of Eqs. (11) and (12).

We start by solving the following general equation:

$$\begin{aligned}\langle W\rangle &= 2\Gamma\int_0^1 [A_d\rho^2 + B_s\rho^4 + B_s\rho^6]\exp(-\gamma\rho^2)\rho\mathrm{d}\rho \\ &= 2\Gamma\left(\int_0^1 A_d\rho^2\exp(-\gamma\rho^2)\rho\mathrm{d}\rho + \int_0^1 B_s\rho^4\exp(-\gamma\rho^2)\rho\mathrm{d}\rho\right. \\ &\quad \left. + \int_0^1 B_s\rho^6\exp(-\gamma\rho^2)\rho\mathrm{d}\rho\right) = 2\Gamma(A_d\alpha + A_s\eta + B_s\xi),\end{aligned} \tag{A1}$$

where

$$\alpha = \int_0^1 \rho^3\exp(-\gamma\rho^2)\mathrm{d}\rho, \tag{A2}$$

$$\eta = \int_0^1 \rho^5\exp(-\gamma\rho^2)\mathrm{d}\rho, \tag{A3}$$

$$\xi = \int_0^1 \rho^7\exp(-\gamma\rho^2)\mathrm{d}\rho. \tag{A4}$$

From Eq. (A1),

$$\langle W\rangle^2 = 4\Gamma^2(A_d^2\alpha^2 + 2A_dA_s\alpha\eta + 2A_dB_s\alpha\xi + \ldots), \tag{A5}$$

where, following Eq. (9), the only important terms are those related with A_d.

Now, Eq. (12) can be written as

$$\begin{aligned}\langle W^2\rangle &= 2\Gamma\int_0^1 [A_d^2\rho^4 + A_dA_s\rho^6 + A_dB_s\rho^8 + \ldots]\exp(-\gamma\rho^2)\rho\mathrm{d}\rho \\ &= 2\Gamma\left(\int_0^1 A_d^2\rho^5\exp(-\gamma\rho^2)\mathrm{d}\rho\right. \\ &\quad + \int_0^1 2A_dA_s\rho^7\exp(-\gamma\rho^2)\mathrm{d}\rho \\ &\quad \left. + \int_0^1 2A_dB_s\rho^9\exp(-\gamma\rho^2)\mathrm{d}\rho + \ldots\right) \\ &= 2\Gamma(A_d^2\eta + 2A_dA_s\xi + 2A_dB_s\tau + \ldots),\end{aligned} \tag{A6}$$

with

$$\tau = \int_0^1 \rho^9 \exp(-\gamma\rho^2)\mathrm{d}\rho. \tag{A7}$$

Thus, following Eqs. (9) and (A2)–(A7),

$$\frac{\partial(\langle W^2\rangle - \langle W\rangle^2)}{\partial A_d} = \frac{\partial(2\Gamma(A_d^2\eta + 2A_dA_s\xi + 2A_dB_s\tau + \ldots))}{\partial A_d} + \frac{\partial(-4\Gamma^2(A_d^2\alpha^2 + 2A_dA_s\alpha\eta + 2A_dB_s\alpha\xi + \ldots))}{\partial A_d} = 0, \tag{A8}$$

resulting in the expression

$$A_d = \frac{A_s(\xi - 2\Gamma\alpha\eta) + B_s(\tau - 2\Gamma\alpha\xi)}{2\Gamma\alpha^2 - \eta}. \tag{A9}$$

The integrals in Eqs. (A2)–(A4) and (A7) can be solved using the recursive form:

$$[n+1] = -\frac{d[n]}{d\gamma}, \tag{A10}$$

defining $\alpha = [1]$, $\eta = [2]$, $\xi = [3]$, and $\tau = [4]$; and

$$[n] = \int_0^1 \rho^{2n+1} \exp(-\gamma\rho^2)\mathrm{d}\rho. \tag{A11}$$

Thus,

$$[0] = \frac{1}{2}\gamma^{-1} - \exp(-\gamma)\left(\frac{1}{2}\gamma^{-1}\right). \tag{A12}$$

Then, using Eqs. (A10) and (A12),

$$\alpha = \frac{1}{2}\gamma^{-2} - \exp(-\gamma)\left(\frac{1}{2}\gamma^{-1} + \frac{1}{2}\gamma^{-2}\right), \tag{A13}$$

$$\eta = \gamma^{-3} - \exp(-\gamma)\left(\frac{1}{2}\gamma^{-1} + \gamma^{-2} + \gamma^{-3}\right), \tag{A14}$$

$$\xi = 3\gamma^{-4} - \exp(-\gamma)\left(\frac{1}{2}\gamma^{-1} + \frac{3}{2}\gamma^{-2} + 3\gamma^{-3} + 3\gamma^{-4}\right), \tag{A15}$$

$$\tau = 12\gamma^{-5} - \exp(-\gamma)\left(\frac{1}{2}\gamma^{-1} + 2\gamma^{-2} + 6\gamma^{-3} + 12\gamma^{-4} + 12\gamma^{-5}\right). \tag{A16}$$

It is interesting to show that, when γ approaches zero, the values of these integrals are $\alpha_{\gamma=0} = 1/4$, $\eta_{\gamma=0} = 1/6$, $\xi_{\gamma=0} = 1/8$, and $\tau_{\gamma=0} = 1/10$; these values can be obtained taking into account that

$$\exp(-\gamma) = 1 - \gamma + \frac{\gamma^2}{2} - \frac{\gamma^3}{6} + \frac{\gamma^4}{24} + \ldots \tag{A17}$$

Funding. Fundación Séneca de la Región de Murcia (15312/PI/10).

Acknowledgment. The authors thank María Luisa López-Ibáñez, Alfonso Navarro, and Jayoung Nam for their comments on mathematical aspects of the text.

REFERENCES

1. P. Jacquinot and B. Roizen-Dossier, *Progress in Optics* (North-Holland, 1964), Vol. **III**.
2. J. Jia, C. Zhou, and L. Liu, "Superresolution technology for reduction of the far-field diffraction spot size in the laser free-space communication system," Opt. Commun. **228**, 271–278 (2003).
3. S. A. Self, "Focusing of spherical Gaussian beams," Appl. Opt. **22**, 658–661 (1983).
4. P. Nisenson and C. Papaliolios, "Detection of earth-like planets using apodized telescopes," Astrophys. J. Lett. **548**, L201–L205 (2001).
5. V. N. Mahajan, *Aberration Theory Made Simple* (SPIE, 1991).
6. M. Born and E. Wolf, *Principles of Optics* (Pergamon, 1965).
7. W. S. Stiles and B. H. Crawford, "The luminous efficiency of rays entering the eye pupil at different points," Proc. R. Soc. London Ser. B **112**, 428–450 (1933).
8. A. Ivanoff, "About the spherical aberration of the eye," J. Opt. Soc. Am. **46**, 901–903 (1956).
9. R. Xu, A. Bradley, and L. N. Thibos, "Impact of primary spherical aberration, spatial frequency and Stiles Crawford apodization on wavefront determined refractive error: a computational study," Ophthalmic Physiol. Opt. **33**, 444–455 (2013).
10. A. Bradley, R. Xu, L. Thibos, G. Marin, and M. Hernandez, "Influence of spherical aberration, stimulus spatial frequency, and pupil apodisation on subjective refractions," Ophthalmic Physiol. Opt. **34**, 309–320 (2014).
11. E. Moreno-Barriuso, J. M. Lloves, S. Marcos, R. Navarro, L. Llorente, and S. Barbero, "Ocular aberrations before and after myopic corneal refractive surgery: LASIK-induced changes measured with laser ray tracing," Invest. Ophthalmol. Vis. Sci. **42**, 1396–1403 (2001).
12. T. Seiler, M. Kaemmerer, P. Mierdel, and H. E. Krinke, "Ocular optical aberrations after photorefractive keratectomy for myopia and myopic astigmatism," Arch. Ophthalmol. **118**, 17–21 (2000).
13. J. T. Holladay, D. R. Dudeja, and J. Chang, "Functional vision and corneal changes after laser in situ keratomileusis determined by contrast sensitivity, glare testing, and corneal topography," J. Cataract Refract. Surg. **25**, 663–669 (1999).
14. N. Lopez-Gil, S. C. Peixoto-de-Matos, L. N. Thibos, and J. M. Gonzalez-Meijome, "Shedding light on night myopia," J. Vis. **12**(5):4, 1–9 (2012).
15. V. N. Mahajan, "Strehl ratio of a Gaussian beam," J. Opt. Soc. Am. A **22**, 1824–1833 (2005).
16. W. B. Wetherell, "The use of image quality criteria in designing a diffraction limited large space telescope," Proc. SPIE **0028**, 45–80 (1972).
17. N. Lopez-Gil and V. Fernandez-Sanchez, "The change of spherical aberration during accommodation and its effect on the accommodation response," J. Vis. **10**(13):12, 1–15 (2010).
18. T. O. Salmon and C. van de Pol, "Normal-eye Zernike coefficients and root-mean-square wavefront errors," J. Cataract Refract. Surg. **32**, 2064–2074 (2006).
19. L. N. Thibos, X. Hong, A. Bradley, and R. A. Applegate, "Accuracy and precision of objective refraction from wavefront aberrations," J. Vis. **4** (4), 329–351 (2004).
20. WolframAlpha Computational knowledge engine, http://www.wolframalpha.com/ (2009).
21. S. Marcos, S. Barbero, L. Llorente, and J. Merayo-Lloves, "Optical response to LASIK surgery for myopia from total and corneal aberration measurements," Invest. Ophthalmol. Vis. Sci. **42**, 3349–3356 (2001).
22. X. Zhang, M. Ye, A. Bradley, and L. Thibos, "Apodization by the Stiles-Crawford effect moderates the visual impact of retinal image defocus," J. Opt. Soc. Am. A **16**, 812–820 (1999).
23. R. A. Applegate and V. Lakshminarayanan, "Parametric representation of Stiles-Crawford functions: normal variation of peak location and directionality," J. Opt. Soc. Am. A **10**, 1611–1623 (1993).
24. R. Xu, A. Bradley, N. Lopez Gil, and L. N. Thibos, "Modelling the effects of secondary spherical aberration on refractive error, image quality and depth of focus," Ophthalmol. Physiol. Opt. **35**, 28–38 (2015).
25. Y. Benard, N. Lopez-Gil, and R. Legras, "Subjective depth of field in presence of 4th-order and 6th-order Zernike spherical aberration

using adaptive optics technology," J. Cataract Refract. Surg. **36**, 2129–2138 (2010).
26. Y. Benard, N. Lopez-Gil, and R. Legras, "Optimizing the subjective depth-of-focus with combinations of fourth- and sixth-order spherical aberration," Vis. Res. **51**, 2471–2477 (2011).
27. N. Lopez-Gil, F. J. Rucker, L. R. Stark, M. Badar, T. Borgovan, S. Burke, and P. B. Kruger, "Effect of third-order aberrations on dynamic accommodation," Vis. Res. **47**, 755–765 (2007).
28. P. S. Kollbaum, A. Bradley, and L. N. Thibos, "Comparing the optical properties of soft contact lenses on and off the eye," Optom. Vis. Sci. **90**, 924–936 (2013).
29. L. Llorente, S. Barbero, J. Merayo, and S. Marcos, "Total and corneal optical aberrations induced by laser in situ keratomileusis for hyperopia," J. Refract. Surg. **20**, 203–216 (2004).
30. P. B. Kruger, N. Lopez-Gil, and L. R. Stark, "Accommodation and the Stiles-Crawford effect: theory and a case study," Ophthalmic Physiolog. Opt. **21**, 339–351 (2001).
31. W. J. Benjamin and I. M. Borish, *Borish's Clinical Refraction*, 2nd ed. (Butterworth-Heinemann, 2006).
32. X. Cheng, A. Bradley, S. Ravikumar, and L. N. Thibos, "Visual impact of Zernike and Seidel forms of monochromatic aberrations," Optom. Vis. Sci. **87**, 300–312 (2010).
33. D. A. Atchison, D. H. Scott, N. C. Strang, and P. Artal, "Influence of Stiles-Crawford apodization on visual acuity," J. Opt. Soc. Am. A **19**, 1073–1083 (2002).
34. D. A. Atchison, A. Joblin, and G. Smith, "Influence of Stiles-Crawford effect apodization on spatial visual performance," J. Opt. Soc. Am. A **15**, 2545–2551 (1998).
35. N. López-Gil, V. Fernández-Sánchez, L. N. Thibos, and R. Montés-Micó, "Objective amplitude of accommodation computed from optical quality metrics applied to wavefront outcomes," J. Optom. **2**, 223–234 (2009).
36. L. Zheleznyak, H. Jung, and G. Yoon, "Impact of pupil transmission apodization on presbyopic through-focus visual performance with spherical aberration," Invest. Ophthalmol. Vis. Sci. **55**, 70–77 (2014).
37. S. Ravikumar, L. N. Thibos, and A. Bradley, "Calculation of retinal image quality for polychromatic light," J. Opt. Soc. Am. A **25**, 2395–2407 (2008).
38. X. Cheng, A. Bradley, and L. N. Thibos, "Predicting subjective judgment of best focus with objective image quality metrics," J. Vis. **4**(4), 310–321 (2004).
39. J. Martin, B. Vasudevan, N. Himebaugh, A. Bradley, and L. Thibos, "Unbiased estimation of refractive state of aberrated eyes," Vis. Res. **51**, 1932–1940 (2011).